Double Charge Transfer Dominates in Carrier Localization in Low Bandgap Sites of Heterogeneous Lead Halide Perovskites

Azhar Fakharuddin,* Marius Franckevičius, Andrius Devižis, Andrius Gelžinis, Jevgenij Chmeliov, Paul Heremans, and Vidmantas Gulbinas*

Heterogeneous organic-inorganic halide perovskites possess inherent non-uniformities in bandgap that are sometimes engineered and exploited on purpose, like in quasi-2D perovskites. In these systems, charge carrier and excitation energy migration to lower-bandgap sites are key processes governing luminescence. The question, which of them dominates in particular materials and under specific experimental conditions, still remains unanswered, especially when charge carriers comprise excitons. In this study transient absorption (TA) and transient photoluminescence (PL) techniques are combined to address the excited state dynamics in quasi-2D and other heterogeneous perovskite structures in broad temperature range, from room temperature down to 15 K. The data provide clear evidence that charge carrier transfer rather than energy migration dominates in heterogeneous quasi-2D perovskite films.

Dr. A. Fakharuddin
Department of physics
University of Konstanz
D-78464 Konstanz, Germany
E-mail: azhar-fakhar.uddin@uni-konstanz.de

Dr. A. Fakharuddin, Prof. P. Heremans
imec
Kapeldreef 75, Leuven 3001, Belgium

Dr. M. Franckevičius, Dr. A. Devižis, Dr. A. Gelžinis, Dr. J. Chmeliov,
Prof. V. Gulbinas
Department of Molecular Compound Physics
Center for Physical Sciences and Technology
Vilnius LT-10257, Lithuania
E-mail: vidmantas.gulbinas@ftmc.lt

Dr. A. Gelžinis, Dr. J. Chmeliov, Prof. V. Gulbinas
Institute of Chemical Physics
Faculty of Physics
Vilnius University
Sauletekio Av. 9, Vilnius LT-10222, Lithuania

Prof. P. Heremans
Department of Electrical Engineering
KU Leuven
Kasteelpark Arenberg, Leuven 3001, Belgium

The ORCID identification number(s) for the author(s) of this article
can be found under https://doi.org/10.1002/adfm.202010076.

1. Introduction

Perovskite films used in solar cells or light emitting diodes (LEDs) are intrinsically heterogeneous.[1,2] They typically consist of grains, that are of different sizes, have varying surface and/or bulk defect numbers, and exhibit different interactions with other grains. The heterogeneity is particularly large when perovskite films contain nanoparticles or other low-dimensional structures where spatial confinement changes the state energies. Electronic processes in such heterogeneous systems are determined not only by excitation dynamics in individual crystallites, but also by migration of charge carriers and/or excitons between heterogeneous sites. When carrier or exciton energies differ between neighboring sites, the migration processes are directed toward lower energy sites. This causes localization of charge carriers and excitons in low-energy sites, especially at low temperatures.

Quasi-2D perovskites represent such strongly heterogeneous systems. They consist of 2D perovskite layers with ABX_3 crystal structure separated by layers of a large (2D) cation spacer. The number of 2D perovskite sheets between organic spacer layers, which can vary from 1 to infinity, defines the so-called n value. Experimentally, this is achieved by varying the stoichiometry of initial precursors forming perovskite thin films, and the resultant perovskite film represents an ensemble of mixed 2D and 3D domains.[3–5] Due to the mixed phase nature of the resultant perovskite film and spatial confinement therein, different structures have different bandgaps and absolute energetic positions of conduction and valence bands. Additional heterogeneity may appear in perovskite films containing mixed halide cations (I, Cl, Br) due to their segregation, creating non-uniform spatial distribution of different halide ions, which in turn results in non-uniform distribution of bandgaps.

Different perovskite structures are also characterized by different exciton binding energies. The exciton binding energy in 3D $CH_3NH_3PbI_3$ (MAPI) is low, of $\approx$5–20 meV,[6–8] therefore the majority of charge carriers at room temperature are not bound to comprise excitons.[9] Larger binding energy of $\approx$40 meV was evaluated for $MAPBr_3$ perovskites.[10] Exciton binding energies in 2D perovskites are of the order of hundreds of meV,[2,11,12] consequently the majority of charge carriers in these structures are expected to be bound in excitons. Therefore, efficient charge carrier generation and their mobility still

remain important issues limiting performance efficiency of solar cells utilizing 2D perovskites.[13]

In perovskites, both exciton and charge carrier migration may take place. The heterogeneity drives charge carrier and exciton localization in sites where their energies are low. In case of MAPI and similar perovskites, where free charge carriers rather than excitons are dominating species, the migration processes are determined by transfer of electrons and holes. On the other hand, at low temperatures and in perovskite structures with a larger exciton binding energy where charge carriers are bound to form excitons, the exciton diffusion may dominate. If the material is composed of distinct domains with different bandgaps and with different band positions on the absolute energy scale, excitons may split when one of the charge carriers is transferred to the neighboring domain with energetically lower states or trapped into trap states.[1,11] These processes lead to generation of free charge carriers or interfacial charge transfer states. Nonetheless, the counter-charge may also be transferred to the same domain if the energy level positions are favorable, thus recreating neutral excitonic state. The final state in this case is identical to the one created during the pure excitonic energy transfer process. However, properties of the both transfer scenarios may be significantly different, showing different dependences on internal perovskite properties and external conditions.

Excitation energy transfer has been suggested to occur between 2D perovskite layers with different sheet numbers.[6,14–16] On the contrary, Shang et al.[17] and Liu et al.[18] concluded that electron and hole transfer is the key process in such a system. Particularly, Liu et al. came to the conclusion that charge carriers tend to separate in mixed quasi-2D perovskites, when electrons localize in the thickest 2D layers while holes diffuse to thin layers.[18] Similar conclusion that charge transfer is the dominant mechanism for energy funneling was also recently reported for the $FAPbBr_3/FAPb(Br_xI_{1-x})_3/FAPbI_3$ microplate sandwich.[19] Zhou et al. concluded that both mechanisms take place: energy transfer between layers dominates on the sub-ns time scale whereas electron transfer occurs at later times.[20]

Consequences of exciton and charge transfer are expected to differ significantly, leading to different optical and electrical response of the material. For example, exciton migration rather than carrier transport may take place between electrically isolated domains. Charge carrier migration may lead to the luminescence quenching if electron and hole tend to localize in different perovskite domains. Charge transfer also causes generation of free charge carriers participating in photocurrent. Consequently, this difference may be important for the device performance, when such materials are used in, for example, solar cells or LEDs. Thin layers of these quasi-2D perovskites deposited on top of 3D perovskite were demonstrated to increase the long-term stability of solar cells;[21,22] however, their influence on the carrier transport is still under debate. Therefore, it is important to clearly understand the exciton/charge carrier migration and localization properties that, as was mentioned, are still largely unknown.

To shed some light on these still unclear processes, we performed ultrafast transient absorption (TA) and time-resolved photoluminescence (PL) experiments at room and low temperatures and investigated the excited state dynamics of conventional 3D MAPI perovskites, as well as mixed (2D)/(3D) polymorphs of MAPI and $CH_3NH_3PbI_2Br_1$ ($MAPI_2Br_1$). We demonstrate that comparison between TA and PL data is a good tool to distinguish between charge carrier and exciton transfer processes. Exciton transfer causes decay of TA and PL signatures of donors and simultaneous growth of those of acceptor. Such processes reveal identical transients in both TA and PL measurements. Contrarily, transfer of just a single charge carrier causes decay of the donor PL without the appearance of acceptor PL, while TA reveals bleaching of the acceptor absorption together with the partial recovery of the donor absorption. However, consequences of the charge and exciton transfer become identical again after transfer of opposite charge.

We demonstrate that double charge transfer dominates in all investigated materials. Moreover, as charge transfer requires thermal activation, one can expect to detect a significant temperature dependence of this process. Indeed, we observe sequential electron and hole transfer in quasi-2D perovskites at high temperatures, reduction of the transfer efficiency of one charge carrier type when temperature decreases, and impeded transfer of both charge carriers at very low temperatures.

2. Results

2.1. MAPI

We start discussion of the exciton/charge carrier transfer processes in a prototypical MAPI film because it is the best-studied perovskite material and thus, serves as a reference in our study. Typical MAPI film formation procedures yield films composed of domains with the sizes of multiple tens to hundreds of nanometers. Top and bottom plots of **Figure 1** show TA and transient PL spectra at different delay times, obtained at different temperatures. The TA spectra show bleaching of the absorption band edge due to the band filling and also reveal a short wavelength bleaching band related to the higher energy transitions.[23] Because of the low exciton binding energy, at low excitation intensities, the majority of charge carriers in 3D MAPI do not form excitons at room temperature and probably at temperatures down to the phase transition.[9] Thus, the observed processes at room and 233 K temperatures must be attributed to free electrons and holes. The room temperature and 233 K data show that the initial absorption bleaching and PL spectra are broadened to the short wavelength side. Spectral narrowing dominantly takes place on a sub-nanosecond time scale, indicating that carrier migration and localization in domains with lower bandgaps take place during hundreds of picoseconds. It is noteworthy that the PL intensity strongly increases at low temperatures. Such increase was reported in literature[24,25] and was explained by temperature dependence of the radiative band-to-band recombination due to Coulomb correlations. Both TA and PL spectra shift to the long wavelength side by reducing temperature from 300 K to 230 K. Similar shift of the PL band has been reported previously and attributed to the anomalous Varshni trend.[26,27]

The film becomes much more heterogeneous at low temperatures, below tetragonal (Tg) to orthorhombic (Or) phase transition taking place at ≈160 K.[27–29] Because of incomplete phase transition, MAPI films at low temperatures possess residual Tg phases in addition to the dominating Or phase.[27,30] The Or phase has larger bandgap and shows PL at ≈730–750 nm.[7,27,29] The initial TA spectrum (0 ps) at 15 K shows no bleaching of the Tg phase (750–800 nm), indicating that the Or phase is strongly
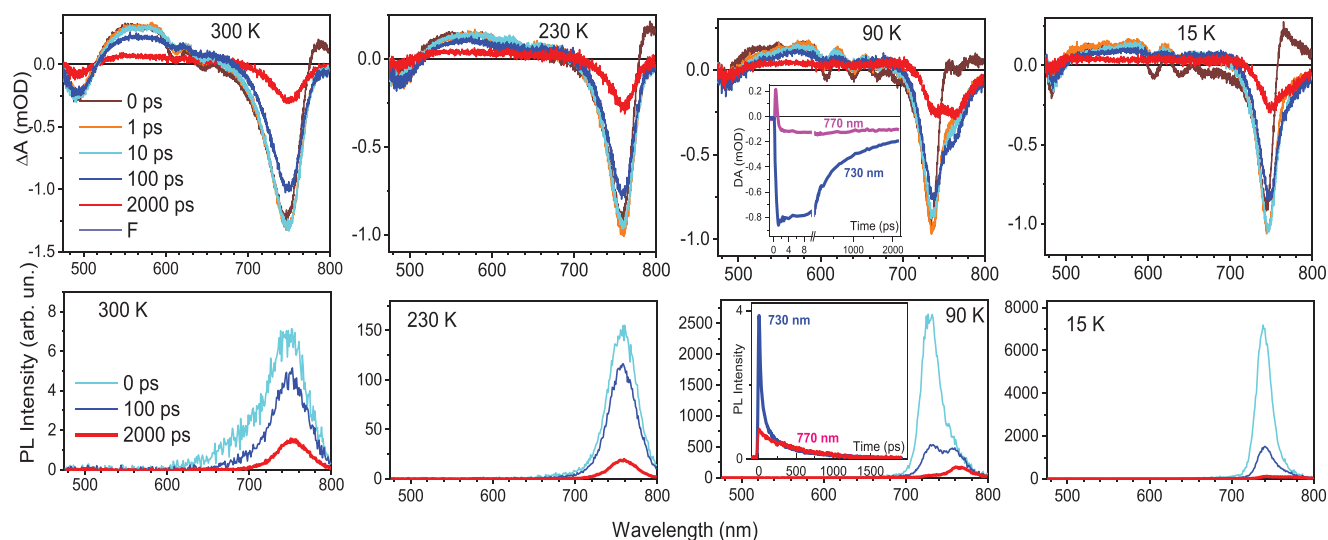
3D MAPI

Figure 1. Time-resolved TA (top figures) and transient PL spectra of 3D MAPI film at different temperatures (excitation wavelength $\lambda_{ex} = 345$ nm). Insets show TA and PL kinetics, respectively, at different wavelengths at 90 K temperature.

dominating and thus, dominantly excited. The 0 ps spectrum at 90 K still shows a weak Tg band, which competes with the induced absorption band of the Or phase. Absorption bleaching of the Tg phase clearly appears within ≈1 ps when energy/charge transfer from photoexcited Or phase takes place (See inset in Figure 1). PL spectra also clearly show Or and Tg components at 90 K. Importantly, PL band of the Or phase decays much faster than the corresponding absorption bleaching. Consequently, the long-living excited state, that forms at 2 ns, causes bleaching of the Or absorption band, but shows no PL. This behavior suggests that only one kind of charge carrier remains after 2 ns in Or domains indicating that one kind of charge carrier is transferred more efficiently. The Tg component completely disappears from the PL spectrum at 15 K, while TA spectrum still shows the long wavelength shoulder attributable to the Tg phase. This is an indication that only one kind of charge carriers and only partly is transferred from Or phase to Tg phase at 15 K. Charge transfer may require thermal assistance, if it takes place over some energy barrier, thus it is not surprising that transfer of one kind of charge carriers stops at very low temperatures. Although charge carriers are expected to form excitons at low temperatures, these experimental data cannot be explained by the exciton transfer. Exciton transfer would lead to identical absorption bleaching and PL kinetics and would not cause formation of non-radiative states. Exciton transfer is also typically much less sensitive to temperature; therefore we would expect to observe exciton transfer from Or to Tg phase and the Tg phase luminescence at 15 K. Consequently, these considerations lead to a conclusion that charge transfer rather than exciton transfer takes place between excited Or and Tg phases at 15 K. At 90 K we do observe PL of the Tg phase indicating that at least fraction of another kind of charge carriers is also transferred. Charge carriers are expected to form excitons at low temperatures, thus transfer of only one charge carrier also means splitting of exciton. Notably, we did not observe a phase transition in the case of mixed halide perovskite (MAPbI$_2$Br$_1$, Figure S5, Supporting Information).

2.2. Quasi-2D MAPI

Quasi-2D perovskites composed of mixtures of 2D perovskites with different sheet numbers (*n* value) together with residual 3D grains represent more heterogeneous perovskite systems. **Figure 2** shows TA and PL spectra of quasi-2D MAPI film with 10% of methylammonium (MA) substituted with butylammonium (BA). At this relatively small substitution level, 2D structures are formed together with residual 3D domains. We can clearly distinguish narrow 2D absorption bleaching band at ≈600 nm and a broadband at ≈750 nm due to 3D domains. The 600 nm band has been attributed to 2D layers composed of three (*n* = 3) perovskite sheets.[6,11,31] Two low intensity bands at ≈570 and 640 nm have been attributed to 2D layers with two and four sheets, respectively. Luminescence spectra are significantly broadened, probably due to exciton-phonon interaction, preventing resolution of different species at room temperature. However, at low temperatures, we can clearly distinguish PL bands of 2D and 3D domains at ≈600 and 700 nm respectively. Attribution of the band in the 650–720 nm region is less straightforward, particularly when absorption bleaching in this spectral region is almost absent. Similar PL properties revealing bands with very large Stokes shifts have been reported for 2D perovskite species and attributed to the self-trapped excitons formed at grain surfaces and interfaces where exciton-phonon coupling causes strong structural deformations.[32] In agreement with this concept, we observe bleaching of the 600 nm band and corresponding luminescence at ≈700 nm. The absence of the negative TA signal in the 650–720 nm region indicates that stimulated emission contributes little to the TA signal. The self-trapping phenomenon falls outside the scope of the present work, therefore we will not analyze it in more detail. We just consider that the 700 nm PL band belongs to the 2D structures. The PL spectra dynamics clearly shows gradual localization of charge carriers in species with low bandgap at room temperature, which stops at low temperatures.
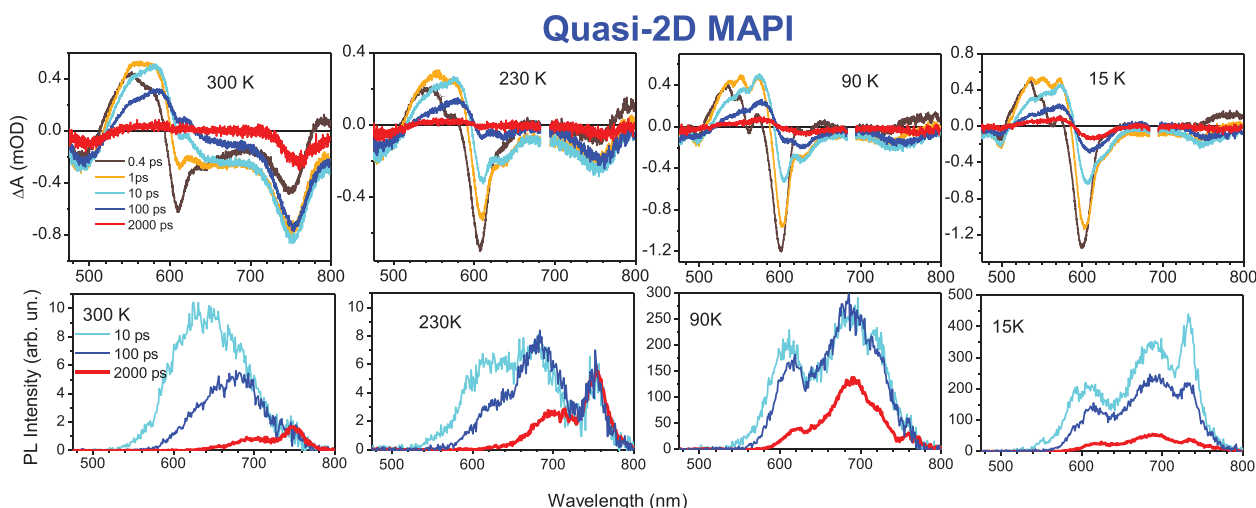
Figure 2. Time-resolved TA (top figures) and transient PL spectra of quasi-2D MAPI (employing 10% BA) film at different temperatures (λ_{ex} = 345 nm). Numerical values on the vertical axes reflect the observed differences in the TA and especially PL intensities at different temperatures.

Figure 3 shows TA kinetics of quasi-2D MAPI at 600 and 750 nm, roughly corresponding to the maxima of absorption bleaching bands of 2D and 3D species, respectively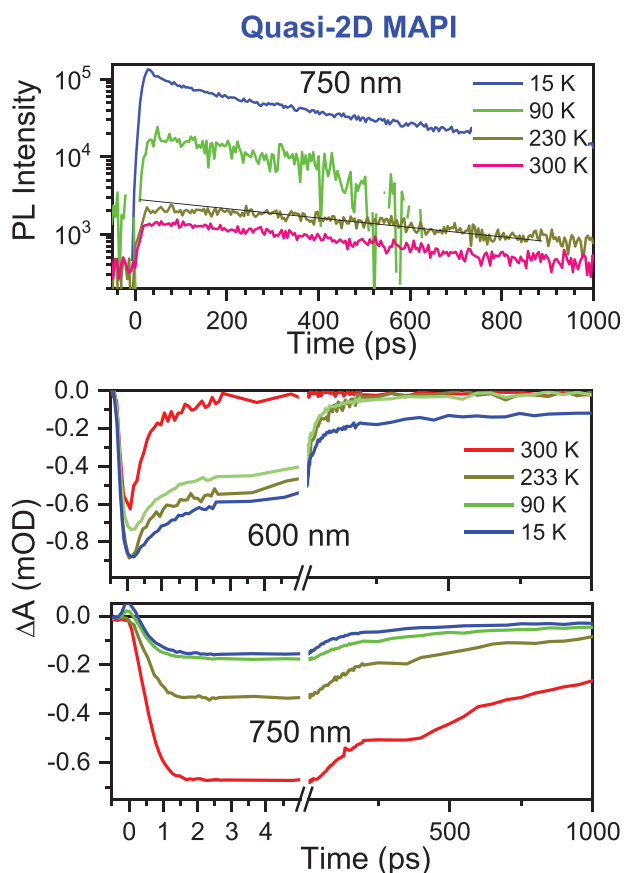. At room temperature, we observe instantaneous (limited by time-resolution of our measurement setup) appearance of the 600 nm absorption bleaching band attributable to 2D species. The 600 nm absorption bleaching band dominantly decays during several ps. Simultaneously, we observe the delayed appearance of the absorption bleaching band at 750 nm indicating energy/charge transfer from 2D to 3D species. At 233 K and lower temperatures, the decay of the 600 nm absorption bleaching band becomes clearly bi-componential. The absorption bleaching decays only partially during the initial several ps decay phase suggesting that only approximately half of charge carriers are transferred to 3D species during this time, while the remaining part decays or is transferred during ≈200 ps. Moreover, at very low 15 K temperature, a very slow component, that is almost constant during 2 ns, appears. In agreement with the reduced transfer efficiency, the amplitude of the 750 nm band attributable to 3D species becomes lower at low temperatures. As TA spectra in Figure 2 show, the 750 nm bleaching band becomes very weak at low temperatures. It confirms that the energy/charge transfer becomes less efficient at low temperatures. It should be also noted that 3D species may be also excited directly by excitation light, therefore the weak 750 nm band bleaching may be partly caused by the direct excitation of the 3D domains. Consequently, we cannot exclude that energy/charge transfer between 2D and 3D domains completely stops at very low temperatures.

The observation of bi-componential transfer dynamics straightforwardly leads to its attribution to the double charge transfer, which was also concluded for 3D perovskite between Or and Tg phases. In case of quasi-2D perovskite, we clearly observe the double charge transfer at 230 K and lower temperatures. At room temperature, the slow transfer component apparently also accelerates to several ps, while at 15 K it slows down to more than 1000 ps, or even completely stops. The more hindered carrier transfers in quasi-2D perovskite than in 3D perovskite is not surprising since different domains in this material are separated by organic BA cation layers, creating obstacles for the charge transfer.

Figure 3. Time-resolved luminescence (top plot) and TA kinetics at different probe wavelengths measured for quasi-2D MAPI film (employing 10% BA) at different temperatures.

Time-resolved PL data support the reduced charge transfer efficiency at very low temperatures. Because of lower time-resolution of PL measurements of ≈13 ps, we do not resolve the fast growth component during the first few ps. But the PL kinetics of 3D structures (750 nm) at 230 and 300 K, has a weak, but reproducible growth component during 100–200 ps (see top plot in **Figure 3**, black line shows exponential decay without growing component). This growth component disappears at 15 K, confirming that the transfer processes are strongly hindered or completely stop at very low temperatures.

Additional support for the double charge transfer mechanism comes from the analysis of the temperature dependencies of PL band intensities. Intensities of 600 and 700 nm PL bands attributed to 2D domains with $n = 3$ and self-trapped excitons increase at 90 K more than 20 times in comparison with those at 230 K (note different Y-scales in Figure 2), while TA spectra show very similar dynamics of the 600 nm bleaching band at both temperatures. Such PL increase, as was discussed, is quite expected for 3D species due to strong temperature dependence of the radiative recombination rate of nonbound charge carriers.[24,25] However, exciton binding energies in 2D MAPI structures were reported to be 38, 270, and 220 meV for layers with $n = 1$, $n = 2$, and $n > 2$, respectively,[11] therefore majority of charge carriers are expected to be bound into excitons at 230 K and lower temperatures. Exciton theory does not predict significant temperature dependence of the radiative exciton recombination rate. This temperature dependence may be explained by assuming that majority of charge carriers are rapidly transferred to the 3D domains at high temperatures (during several ps, according to TA data) causing very weak PL.

At low temperatures, the charge transfer rate decreases, more charge carriers remain in the 2D domains, therefore their PL intensity strongly increases.

2.3. Quasi-2D MAPb(I/Br)

To evaluate whether the double charge transfer mechanism is applicable to other quasi-2D perovskites, we investigated quasi-2D MAPb(I/Br) samples with different BA contents. **Figure 4** shows 3D TA and PL plots measured for MAPb(I/Br) films with 10%, 20%, and 50% of BA. TA spectra measured at room temperature (Figure 4), significantly depend on the BA content. In the sample with 10% BA, we observe only weak absorption bleaching bands at ≈580 and 650 nm, attributable to 2D domains with different sheet numbers. These bands almost disappear during hundreds of ps, indicating very fast carrier localization in 3D domains. In samples with higher BA content, the short wavelength bands become stronger because of larger relative content of 2D domains, particularly with low sheet numbers. On the other hand, room temperature PL spectra of all MAPb(I/Br) films are quite similarly dominated by the long wavelength band. It should be noted that 3D MAPb(I/Br) has the lowest energy absorption band at ≈650 nm;[33] however, segregation of I and Br ions causing formation of Br-rich and I-rich domains were often observed.[34–37] The 3D I-rich perovskite domains have similar bandgap as MAPI, while Br-rich 3D domains have PL band at ≈530 nm.[38] Typically, segregation was observed under the material illumination.[39] In case of the investigated quasi-2D samples, we
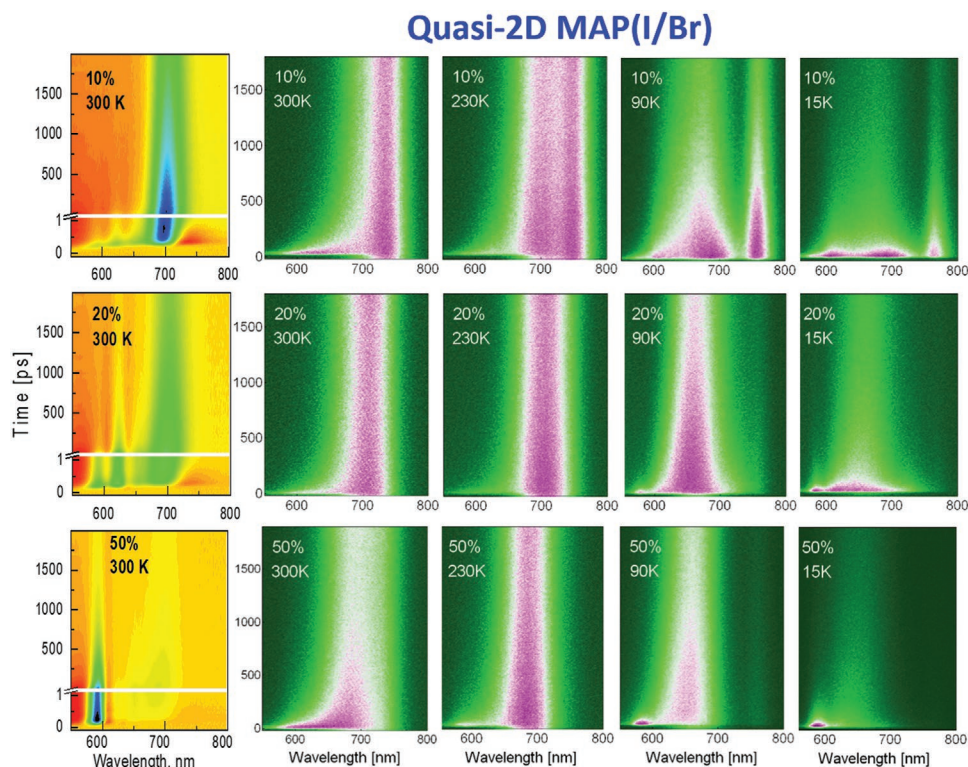

Figure 4. TA evolution for quasi-2D MAPI$_2$Br$_1$ samples with 10%, 20%, and 50% BA contents at room temperature and PL evolutions at different temperatures.

**ADVANCED
SCIENCE NEWS**

www.advancedsciencenews.com
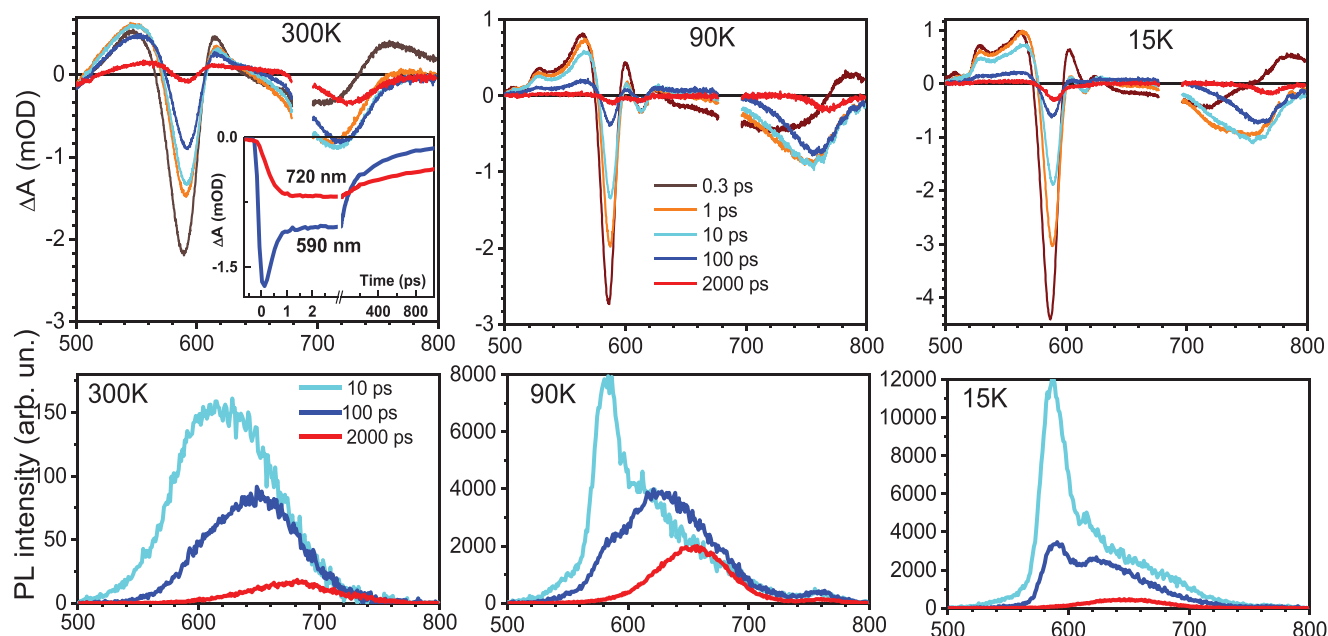
**ADVANCED
FUNCTIONAL
MATERIALS**

www.afm-journal.de

Figure 5. TA (top plots) and time-resolved PL spectra (lower plots) of quasi-2D MAPb(I/Br) film with 50% BA at different temperatures ($\lambda_{ex} = 345$ nm). The inset shows TA kinetics at 300 K temperature at two probe wavelengths. Numerical values on the vertical axes reflect the observed differences in the PL intensities at different temperatures.

have not observed spectra modifications during the PL measurement time, therefore segregation apparently took place already during the film formation or storage, thus the observed PL at $\lambda > 700$ nm should be attributed to I-rich domains. In samples with larger BA content, the PL band slightly shifts to the short wavelength side, which should be attributed to luminescence of 2D I-rich domains with a large sheet number. Importantly, the bleaching band at 580 nm becomes dominates in the sample with 50% BA, while PL spectra reveal no significant difference in this spectral region between different samples. It indicates that the excited species responsible for the 580 nm bleaching band are non-fluorescent, most likely containing only one kind of charge carrier.

At low temperatures, the short-wavelength PL bands attributable to 2D domains, become stronger and even dominating (see right hand plots of Figure 4) indicating that both charge carriers remain in 2D species responsible for the ≈580 nm band. In agreement with the inefficient charge transfer, the long-wavelength spectral component at $\lambda > 700$ nm almost completely disappears at 15 K in the sample with 50% BA.

Figure 5 shows TA and time-resolved PL spectra at different temperatures for the sample with 50% BA (see time-resolved PL of all types of perovskite samples investigated in this study in Figure S4, Supporting Information). The strong absorption bleaching band at ≈590 nm indicates that 2D domains strongly dominate in this sample. At room temperature, this band shows partial decay during several ps (inset in Figure 5), and simultaneously the absorption bleaching at 720 nm growth. In analogy to the quasi-2D MAPI film, we attribute the partial absorption bleaching decay to the transfer of only one type of charge carriers to the 3D domains.

TA and PL spectra show noticeably different behavior at low temperatures: we clearly observe delayed formation of the absorption bleaching band at wavelengths larger than 700 nm due to delayed charge carrier localization in 3D domains, on the other hand, PL of 3D domains is completely absent at 15 K and only very weak at 90 K. This is a clear evidence that only one kind of charge carriers is transferred to the 3D domains at 15 K. It also suggests that we can rule out the energy transfer, which would cause transfer of both types of charge carriers to the 3D domains resulting in their luminescence.

Summarising, we observe three indications that double charge transfer rather than energy transfer dominates in charge carrier localization in perovskite structures with low energy gaps. 1) Carrier localization in domains with a low energy gap becomes less efficient at low temperatures. It indicates that the transfer process requires thermal activation, which is typical for the charge transport in disordered materials, while uncharacteristic for energy transfer. 2) Bi-componential absorption bleaching decays of high energy bands indicating that carriers of one type are transferred to domains with small energy gap faster than another type of carriers. 3) TA reveals formation of long-living non-luminescent states both in 2D and 3D domains at low temperatures, indicating that charge separation between 2D and 3D structures creates non-radiative states.

3. Discussion

A contact of two materials with different energy level positions might result in two types of junctions: type I and type II, as shown in top panel of **Figure 6**. Majority of recent publications

**ADVANCED
SCIENCE NEWS**
www.advancedsciencenews.com

**ADVANCED
FUNCTIONAL
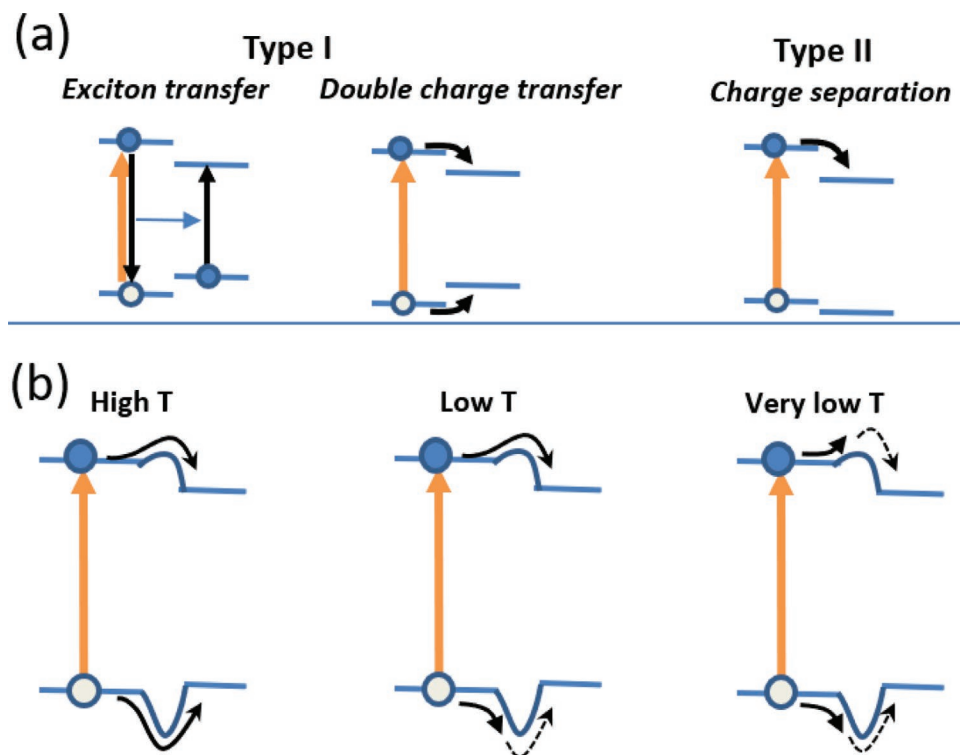MATERIALS**
www.afm-journal.de

Figure 6. a) Electronic processes in Type I and Type II heterojunctions. Schemes (b) show Type I heterojunctions formed between perovskite domains with different bandgaps accounting for barriers for the charge transfer. At room temperature, transfer of both electrons and holes takes place as the thermal energy is sufficient to cross barriers. At low temperatures (90 < T < 230 K) the hole transfer slows down causing temporal charge separation, while at very low temperatures (T = 15 K) transfer of both electron and hole becomes hampered. This leads to a strong emission from local 2D domains and a weak emission from 3D domains, as is experimentally shown in Figures 3, 5, and 6.

consider that quasi-2D perovskites with different layer numbers n form Type I structures.[14–16,40,41] These assignments were mainly based on observation of gradual redistribution of luminescence originating from low-n to large-n domains. On the other hand, Type II heterojunctions were also suggested, where authors considered that hole localization takes place in domains with low-n and electrons in domains with high-n.[17,18] Our experimental results also suggest that type I heterojunctions are formed in the investigated samples. Generally, both exciton and double charge transfer (successive electron and hole transfer) processes may take place in type I heterojunctions. The double charge transfer in the end also leads to the same final state as exciton transfer, with both electron and hole located in the medium with low bandgap. Our experimental data show that charge transfer processes in investigated perovskite materials strongly depend on temperature, which suggests importance of thermally stimulated exciton splitting or presence of low energy barriers between perovskite domains. These processes slow down at low temperatures and limit transfer rate of one type of charge carrier, while at very low temperatures transfer of both charge carriers become very inefficient.

It is reasonable to expect that the transfer rate correlates with the positions of energy levels. Consequently, there is common agreement that electron energy decreases in domains with large-n while energetic positions of valence band are less clear. Therefore, it is more likely that electron transfer to large-n domains is more energetically favorable and occurs faster than transfer

of holes. Consequently, we associate the fast (several ps) carrier transfer process with electrons. The hole transfer, on the other hand, is less favorable and requires more thermal assistance, therefore it slows down to more than 2 ns at 15 K.

The intermediate states, when only one charge carrier (electron) is transferred, are difficult to detect and investigate, particularly when they are short-lived. General considerations suggest that the transfer of one charge may also stimulate transfer of a countercharge, because the intermediate state creates charged donor and acceptor domains, which leads to adjustment of energy levels. Hardly any experimental technique can distinguish between energy and double charge transfer if both charge carriers are transferred with similar rates or transfer of the countercharge occurs very rapidly after transfer of the first charge carrier. On the other hand, sample cooling, as we demonstrate, may change these transfer rates, leading to a situation when transfer of the second charge becomes much slower, or transfer of both charge carriers becomes significantly hindered at very low temperatures (see Figure 6), thus enabling observation of the charge separated state by means of time-resolved PL and TA techniques. We have recently demonstrated that sample cooling causes dramatic photocurrent changes in conventional 3D MAPI films[42] indicating that energy barriers formed between perovskite grains play an important role in carrier migration. Thus, the presence of energy barriers between perovskite domains, which may be different for electrons and holes, is not surprising.

ADVANCED
SCIENCE NEWS
www.advancedsciencenews.com

ADVANCED
FUNCTIONAL
MATERIALS
www.afm-journal.de

Although both exciton and double charge transfer finally cause carrier localization in low-bandgap states, properties of the two transfer processes may be significantly different, as electron and charge transfer generally differently depend on material properties and external conditions. The two processes may cause important differences in performance of perovskite devices. Performance of solar cells is based on charge separation, thus the sequential charge transfer involving charge separated state plays an important role in solar cells based on 2D perovskites[43–45] as well as in 3D perovskite cells with top 2D-perovskite layer.[22,44] On the other hand, PeLED performance is based on exciton states, thus clear understanding of their formation and transformation processes is also very important for the PeLED development. Future research should focus on systematically controlling charge separation efficiency in these perovskite systems. This can be achieved via dimensionality tailoring to control the heterogeneity spatially, for example, by forming a monodispersed quantum well- like structure[46] that can favor more efficient charge separation and can guide the charges to the perovskite domains with the smallest bandgap.

4. Conclusions

We have investigated localization of photogenerated charge carriers in heterogeneous perovskites composed of domains with different bandgaps formed in conventional MAPI perovskite below incomplete tetragonal-orthorhombic phase transition and in quasi-2D perovskites composed of domains with different sheet numbers. Combination of the time-resolved luminescence and TA investigations at various temperatures allowed us to distinguish between two different transfer processes resulting in the same final state—the transfer of the exciton as a whole, and sequential electron and hole transfer with the intermediate state of the separated charges. We observed clear indications of the sequential electron and hole transfer in quasi-2D perovskites at room and reduced temperatures as well as between different crystalline phases of MAPI. In quasi-2D perovskites, sequential charge transfer causes charge separation between domains with high and low bandgaps leading to the fluorescence quenching, but all transfer processes almost stop at very low, 15 K temperature. The double charge transfer in heterogeneous perovskite materials is an important signpost for better understanding and optimization of complex electrical and optical properties of perovskites.

5. Experimental Section

The perovskite films were prepared using a modified two-step perovskite processing method reported elsewhere.[47] The reference 3D MAPbI perovskite films were made from a 0.3 M PbI_2 solution in a mixture of dimethylformamide and dimethylsulfoxide and 10 mg mL^{-1} of MA iodide (MAI) in isopropanol alcohol. For mixed halide perovskites MAPb(I/Br), a 55:45 molar ratio of MAI to MABr was used.

In the case of mixed phase quasi-2D perovskites, a large cation, for example, BA was incorporated in the 3D perovskite films via adding BA iodide in PbI_2 solution in different percentages (10, 20, and 50% wt%) with respect to the molar concentration of PbI_2. The solution was heated on a hot plate at 60 °C to better dissolve the precursors. The perovskite films were processed on pre-cleaned non-quenching (glass) substrates

in a modified two-step method. In a first step, a warm solution of PbI_2 (kept at 50 °C) was spin coated for 30 s (3000 rpm). In the next step, the second solution containing either MAI or a mixture of MAI/MABr was dropped on the spinning substrate and spun for 30 s (2000 rpm). A subsequent annealing of perovskite films was carried out at 80 °C for 20 min to complete the crystallization process.

Steady state absorption spectra of the perovskite films, measured by using a UV–vis absorption spectrophotometer (Varian, Cary 300) at room temperature are presented in Supporting Information Figure S1, Supporting Information. The spectra of quasi-2D samples do not explicitly reveal characteristic bands of 2D perovskites, because all samples represent mixtures 2D-perovskites with different sheet numbers n. Additional modifications of MAPb(I/Br) sample spectra may be caused by the halide cation segregation. XRD spectra presented in Figure S2, Supporting Information clearly show additional bands formed in quasi-2D samples.

Time-resolved PL investigations were performed by means of Hamamatsu Streak camera operating in a single sweep regime. Femtosecond Yb:KGW laser (Light Conversion Ltd.) producing 80 fs, 1030 nm light pulses at a repetition rate of 76 MHz was employed for the sample excitation. Third harmonics beam of the femtosecond laser (345 nm) (generated by HIRO harmonics generator, Light Conversion Ltd.) used for excitation was focused into a ≈30 μm spot on the sample. Excitation power density was attenuated using neutral density filters to ≈250 mW cm^{-2}. The time resolution of the entire system was ≈13 ps. In case of PL lifetimes longer than time interval between excitation pulses, the spectra were corrected mathematically to remove contribution of the luminescence created by previous pulses.

TA investigations (Figure S3, Supporting Information) were performed via an amplified femtosecond laser Pharos (10-600-PP, Light Conversion Ltd.), operating at fundamental wavelength of 1032 nm, repetition rate of 200 kHz, and pulse width of <250 fs. The excitation wavelength was chosen at 345 nm, identical as for transient PL measurements via a collinear optical parametric amplifier Orpheus PO15F2L (Light Conversion Ltd.). The measurements were performed at repetition rate of 4.762 kHz frequency achieved by using the pulse picker. Excitation was modulated at 0.794 kHz frequency by mechanical chopper synchronized to the output of the pulse picker. For the probe beam, spectrally broadened pulses by means of continuum generation in the sapphire crystal were used. The detection equipment consisted of Andor Shamrock SR-500i-B1-R spectrometer (Andor Technology, 150 lines mm^{-1} diffraction grating) equipped with Andor Newton (Andor Technology) DU970 CCD camera (1600 × 200 pixels). The reading of the camera was synchronized with the chopper.

A liquid helium cold finger cryostat (Janis CCS-100/204) was used for low temperature PL measurements. The temperature was controlled via a digital temperature controller. Sufficient time was allowed between each temperature step to ensure a stable temperature within the cryostat. It should be noted that the sample properties were reversible during the cooling-heating cycle.

Supporting Information

Supporting Information is available from the Wiley Online Library or from the author.

Acknowledgements

Conflict of Interest

The authors declare no conflict of interest.

Data Availability Statement

Research data are not shared.

Keywords

[1] E. M. Tennyson, T. A. S. Doherty, S. D. Stranks, *Nat. Rev. Mater.* **2019**, *4*, 573.

[2] J. Nishida, A. H. Alfaifi, T. P. Gray, S. E. Shaheen, M. B. Raschke, *ACS Energy Lett.* **2020**, *5*, 1636.

[3] A. Fakharuddin, U. Shabbir, W. Qiu, T. Iqbal, M. Sultan, P. Heremans, L. Schmidt-Mende, *Adv. Mater.* **2019**, *31*, 1807095.

[4] A. B. R. M. Yusoff, M. K. Nazeeruddin, *Adv. Energy Mater.* **2017**, *8*, 1702073.

[5] H. Lin, C. Zhou, Y. Tian, T. Siegrist, B. Ma, *ACS Energy Lett.* **2018**, *3*, 54.

[6] Q. Lin, A. Armin, R. C. R. Nagiri, P. L. Burn, P. Meredith, *Nat. Photonics* **2014**, *9*, 106.

[7] L. M. Herz, *Ann. Rev. Phys. Chem.* **2016**, *67*, 65.

[8] J. M. Frost, K. T. Butler, F. Brivio, C. H. Hendon, M. Van Schilfgaarde, A. Walsh, *Nano Lett.* **2014**, *14*, 2584.

[9] V. D'Innocenzo, G. Grancini, M. J. P. Alcocer, A. R. S. Kandada, S. D. Stranks, M. M. Lee, G. Lanzani, H. J. Snaith, A. Petrozza, *Nat. Commun.* **2014**, *5*, 3586.

[10] F. Ruf, M. F. Aygüler, N. Giesbrecht, B. Rendenbach, A. Magin, P. Docampo, H. Kalt, M. Hetterich, *APL Mater.* **2019**, *7*, 031113.

[11] J.-C. Blancon, H. Tsai, W. Nie, C. C. Stoumpos, L. Pedesseau, C. Katan, M. Kepenekian, C. M. M. Soe, K. Appavoo, M. Y. Sfeir, S. Tretiak, P. M. Ajayan, M. G. Kanatzidis, J. Even, J. J. Crochet, A. D. Mohite, *Science* **2017**, *355*, 1288.

[12] K. Tanaka, T. Kondo, *Sci. Technol. Adv. Mater.* **2003**, *4*, 599.

[13] A. O. El-Ballouli, O. M. Bakr, O. F. Mohammed, *J. Phys. Chem. Lett.* **2020**, *11*, 5705.

[14] N. Wang, L. Cheng, R. Ge, S. Zhang, Y. Miao, W. Zou, C. Yi, Y. Sun, Y. Cao, R. Yang, Y. Wei, Q. Guo, Y. Ke, M. Yu, Y. Jin, Y. Liu, Q. Ding, D. Di, L. Yang, G. Xing, H. Tian, C. Jin, F. Gao, R. H. Friend, J. Wang, W. Huang, *Nat. Photonics* **2016**, *10*, 699.

[15] M. Yuan, L. N. Quan, R. Comin, G. Walters, R. Sabatini, O. Voznyy, S. Hoogland, Y. Zhao, E. M. Beauregard, P. Kanjanaboos, Z. Lu, D. H. Kim, E. H. Sargent, *Nat. Nanotechnol.* **2016**, *11*, 872.

[16] O. F. Williams, Z. Guo, J. Hu, L. Yan, W. You, A. M. Moran, *J. Chem. Phys.* **2018**, *148*, 134706.

[17] Q. Shang, Y. Wang, Y. Zhong, Y. Mi, L. Qin, Y. Zhao, X. Qiu, X. Liu, Q. Zhang, *J. Phys. Chem. Lett.* **2017**, *8*, 4431.

[18] J. Liu, J. Leng, K. Wu, J. Zhang, S. Jin, *J. Am. Chem. Soc.* **2017**, *139*, 1432.

[19] Z. Gan, W. Chen, C. Zhou, L. Yu, L. Dong, B. Jia, X. Wen, *J. Phys. Chem. Lett.* **2020**, *11*, 5963.

[20] N. Zhou, Z. Ouyang, J. Hu, O. F. Williams, L. Yan, W. You, A. M. Moran, *J. Phys. Chem. Lett.* **2020**, *11*, 4570.

[21] K. T. Cho, Y. Zhang, S. Orlandi, M. Cavazzini, I. Zimmermann, A. Lesch, N. Tabet, G. Pozzi, G. Grancini, M. K. Nazeeruddin, *Nano Lett.* **2018**, *18*, 5467.

[22] G. Grancini, C. Roldán-Carmona, I. Zimmermann, E. Mosconi, X. Lee, D. Martineau, S. Narbey, F. Oswald, F. De Angelis, M. Graetzel, M. K. Nazeeruddin, *Nat. Commun.* **2017**, *8*, 15684.

[23] X. Zhu, H. Su, R. A. Marcus, M. E. Michel-Beyerle, *J. Phys. Chem. Lett.* **2014**, *5*, 3061.

[24] R. L. Milot, G. E. Eperon, H. J. Snaith, M. B. Johnston, L. M. Herz, *Adv. Funct. Mater.* **2015**, *25*, 6218.

[25] C. L. Davies, M. R. Filip, J. B. Patel, T. W. Crothers, C. Verdi, A. D. Wright, R. L. Milot, F. Giustino, M. B. Johnston, L. M. Herz, *Nat. Commun.* **2018**, *9*, 293.

[26] Y. P. Varshni, *Physica* **1967**, *34*, 149.

[27] A. Dobrovolsky, A. Merdasa, E. L. Unger, A. Yartsev, I. G. Scheblykin, *Nat. Commun.* **2017**, *8*, 34.

[28] K. P. Ong, T. W. Goh, Q. Xu, A. Huan, *J. Phys. Chem. Lett.* **2015**, *6*, 681.

[29] P. S. Whitfield, N. Herron, W. E. Guise, K. Page, Y. Q. Cheng, I. Milas, M. K. Crawford, *Sci. Rep.* **2016**, *6*, 35685.

[30] C. Wehrenfennig, M. Liu, H. J. Snaith, M. B. Johnston, L. M. Herz, *APL Mater.* **2014**, *2*, 081513.

[31] Y. Lin, Y. Fang, J. Zhao, Y. Shao, S. J. Stuard, M. M. Nahid, H. Ade, Q. Wang, J. E. Shield, N. Zhou, A. M. Moran, J. Huang, *Nat. Commun.* **2019**, *10*, 1008.

[32] X. Wu, M. T. Trinh, D. Niesner, H. Zhu, Z. Norman, J. S. Owen, O. Yaffe, B. J. Kudisch, X. Y. Zhu, *J. Am. Chem. Soc.* **2015**, *137*, 2089.

[33] D. Cui, Z. Yang, D. Yang, X. Ren, Y. Liu, Q. Wei, H. Fan, J. Zeng, S. Liu, *J. Phys. Chem. C* **2016**, *120*, 42.

[34] P. Gratia, G. Grancini, J.-N. Audinot, X. Jeanbourquin, E. Mosconi, I. Zimmermann, D. Dowsett, Y. Lee, M. Grätzel, F. De Angelis, K. Sivula, T. Wirtz, M. K. Nazeeruddin, *J. Am. Chem. Soc.* **2016**, *138*, 15821.

[35] I. L. Braly, R. J. Stoddard, A. Rajagopal, A. R. Uhl, J. K. Katahara, A. K. Y. Jen, H. W. Hillhouse, *ACS Energy Lett.* **2017**, *2*, 1841.

[36] W. Li, M. U. Rothmann, A. Liu, Z. Wang, Y. Zhang, A. R. Pascoe, J. Lu, L. Jiang, Y. Chen, F. Huang, F. Peng, Q. Bao, J. Etheridge, U. Bach, Y.-B. Cheng, *Adv. Energy Mater.* **2017**, *7*, 1700946.

[37] S. J. Yoon, M. Kuno, P. V. Kamat, *ACS Energy Lett.* **2017**, *2*, 1507.

[38] S. Ruan, M.-A. Surmiak, Y. Ruan, D. P. McMeekin, H. Ebendorff-Heidepriem, Y.-B. Cheng, J. Lu, C. R. McNeill, *J. Mater. Chem. C* **2019**, *7*, 9326.

[39] E. M. Hutter, L. A. Muscarella, F. Wittmann, J. Versluis, L. McGovern, H. J. Bakker, Y.-W. Woo, Y.-K. Jung, A. Walsh, B. Ehrler, *Cell Rep. Phys. Sci.* **2020**, *1*, 100120.

[40] Y. Fu, W. Zheng, X. Wang, M. P. Hautzinger, D. Pan, L. Dang, J. C. Wright, A. Pan, S. Jin, *J. Am. Chem. Soc.* **2018**, *140*, 15675.

[41] Q. Ou, X. Bao, Y. Zhang, H. Shao, G. Xing, X. Li, L. Shao, Q. Bao, *Nano Mater. Sci.* **2019**, *1*, 268.

[42] R. Jasiūnas, R. Gegevičius, M. Franckevičius, V. Jašinskas, V. Gulbinas, *Adv. Opt. Mater.* **2020**, *8*, 2000036.

[43] H. Tsai, W. Nie, J.-C. Blancon, C. C. Stoumpos, R. Asadpour, B. Harutyunyan, A. J. Neukirch, R. Verduzco, J. J. Crochet, S. Tretiak, L. Pedesseau, J. Even, M. A. Alam, G. Gupta, J. Lou, P. M. Ajayan, M. J. Bedzyk, M. G. Kanatzidis, A. D. Mohite, *Nature* **2016**, *536*, 312.

[44] D. H. Cao, C. C. Stoumpos, O. K. Farha, J. T. Hupp, M. G. Kanatzidis, *J. Am. Chem. Soc.* **2015**, *137*, 7843.

[45] I. C. Smith, E. T. Hoke, D. Solis-Ibarra, M. D. McGehee, H. I. Karunadasa, *Angew. Chem., Int. Ed.* **2014**, *53*, 11232.

[46] A. H. Proppe, R. Quintero-Bermudez, H. Tan, O. Voznyy, S. O. Kelley, E. H. Sargent, *J. Am. Chem. Soc.* **2018**, *140*, 2890.

[47] A. Fakharuddin, W. Qiu, G. Croes, A. Devižis, R. Gegevičius, A. Vakhnin, C. Rolin, J. Genoe, R. Gehlhaar, A. Kadashchuk, V. Gulbinas, P. Heremans, *Adv. Funct. Mater.* **2019**, *29*, 1904101.